

Listen to Look into the Future: Audio-Visual Egocentric Gaze Anticipation

Bolin Lai¹ Fiona Ryan¹ Wenqi Jia¹ Miao Liu^{2*} James M. Rehg^{1*}

¹Georgia Institute of Technology ²Meta AI

{bolin.lai, fkryan, wenqi.jia, rehg}@gatech.edu miaoliu@meta.com

Abstract

Egocentric gaze anticipation serves as a key building block for the emerging capability of Augmented Reality. Notably, gaze behavior is driven by both visual cues and audio signals during daily activities. Motivated by this observation, we introduce the first model that leverages both the video and audio modalities for egocentric gaze anticipation. Specifically, we propose a Contrastive Spatial-Temporal Separable (CSTS) fusion approach that adopts two modules to separately capture audio-visual correlations in spatial and temporal dimensions, and applies a contrastive loss on the re-weighted audio-visual features from fusion modules for representation learning. We conduct extensive ablation studies and thorough analysis using two egocentric video datasets: Ego4D and Aria, to validate our model design. We also demonstrate our model outperforms prior state-of-the-art methods by at least +1.9% and +1.6%. Moreover, we provide visualizations to show the gaze anticipation results and provide additional insights into audio-visual representation learning.

1. Introduction

A person's eye movements during their daily activities are reflective of their intentions and goals (see [19] for a representative cognitive science study). The ability to predict the future gaze targets of the camera-wearer from egocentric videos, known as *egocentric gaze anticipation*, is therefore a key step towards understanding and modeling cognitive processes and decision making. Furthermore, this capability could enable new applications in Augmented Reality and Wearable Computing, especially in social scenarios - for example, providing memory aids for patients with cognitive impairments, or reducing the latency of content delivery in such AR systems. However, forecasting the gaze fixations of a camera-wearer using only the egocentric view (i.e. without eye tracking at testing time) is very challenging due to the complexity of egocentric scene content and

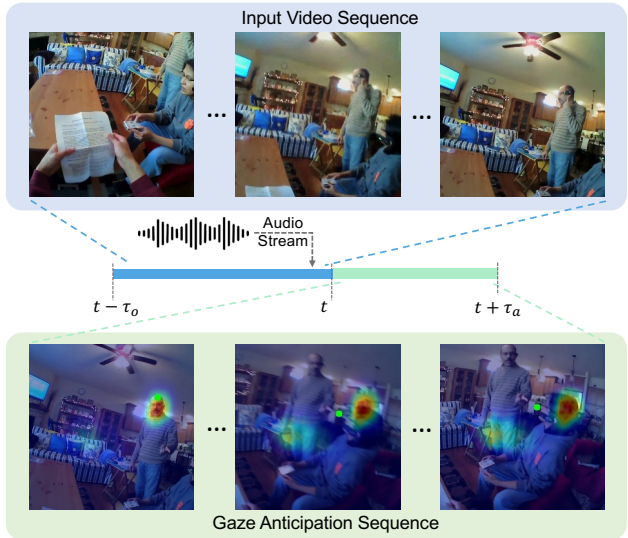


Figure 1. The problem setting of egocentric gaze anticipation. τ_o denotes the observation time, and τ_a denotes the anticipation time. Given the video frames and audio signals of the Input Video Sequence, the model seeks to predict the gaze fixation distribution for the time steps in the Gaze Anticipation Sequence. Green dots indicate the gaze targets in future frames and the heatmap shows the gaze anticipation result from our model.

the dynamic nature of gaze behaviors.

We argue that audio signals can serve as an important auxiliary cue for egocentric gaze forecasting. Consider the example in Fig. 1. During the input video sequence, the camera view shifts from the paper held by the camera wearer to the standing speaker, who asks a question. In the anticipation sequence, the sitting speaker on the far right begins to answer the question and the camera wearer's gaze shifts towards the sitting person's head. The influence of audio signals on eye movements is also evidenced by neuroscience research [50]. Therefore, we address the problem of forecasting the gaze fixation of the camera-wearer in unseen future frames using a short egocentric video clip and corresponding audio. As shown in Fig. 1, the model's ability to fuse the audio and visual cues enables it to correctly

*Equal corresponding author

predict the future attention to the seated subject.

Though several works have addressed egocentric gaze estimation [24–26, 33–35, 54], the problem of egocentric gaze *anticipation* is largely understudied [65]. Moreover, no prior works on egocentric gaze modeling have explored how to leverage the audio modality. Intuitively, in the spatial dimension, the visual region (*e.g.* sound source) that has a stronger correlation with audio signals is more likely to be the potential future gaze target. In the temporal dimension, events in the audio signal may drive both egocentric visual capture (via head movement) and gaze movements as the camera wearer responds to new sounds. Prior approaches for audio-visual representation learning [5–7, 21, 47, 58, 62] directly feed visual and audio embeddings into one multimodal fusion layer. However, such a fusion mechanism is not ideal under the egocentric setting, where the audio signal drives the embodied egocentric visual perception, and thus causes drastic scene change. Therefore, predicting the future gaze behavior demands a model can reason the spatial and temporal relationships between the audio and visual signals in separate.

To this end, we propose a novel Contrastive Spatial-Temporal Separable (CSTS) audio-visual fusion method for egocentric gaze anticipation. Specifically, we input the egocentric video frames and the corresponding audio spectrograms into a video encoder and an audio encoder respectively. Then we leverage self-attention to develop a spatial fusion module and a temporal fusion module in parallel for modeling the spatial and temporal audio-visual correlation separately, strategically highlighting important audio-visual correlations. The output representations from the two branches are merged by channel-wise reweighting and fed into a visual decoder to predict the future gaze target. We use a multi-modal contrastive loss [2] on the reweighted representations from the fusion modules to facilitate audio-visual correspondence learning. We demonstrate the benefits of our approach on two egocentric video datasets that capture social scenarios and everyday activities: Ego4D [17] and Aria [29]. Our proposed model achieves state-of-the-art performance on egocentric gaze anticipation. Our contributions are summarized as follows:

- We introduce the first model that utilizes visual and audio signals for modeling egocentric gaze behaviors.
- We propose a novel CSTS model that leverages a spatio-temporal separable fusion module and a post-fusion contrastive learning schema to facilitate audio-visual representation learning for egocentric gaze anticipation.
- We present comprehensive experiment results on the Ego4D [17] and Aria [29] datasets. Our ablation studies show audio modality can improve the performance by +2.5% and +2.4% in F1 score on Ego4D and Aria. We then show our model also outperforms prior works by at least +1.9% and +1.6% in F1 score on the two datasets.

2. Related Work

Our work relates to three main streams of research: egocentric gaze modeling, audio-visual saliency prediction, and contrastive audio-visual representation learning. It is worth noting that no existing egocentric gaze modeling studies leverage audio signals and previous methods on audio-visual saliency prediction problem are not appropriate for egocentric gaze anticipation as detailed below.

Egocentric Gaze Modeling. Modeling human gaze behavior in egocentric videos is an important topic in egocentric vision. Most prior efforts target egocentric gaze estimation [24–26, 33–35]. Huang *et al.* [24] propose learning temporal attention transitions from video features that reflect drastic gaze movements. Li *et al.* [35] and Huang *et al.* [25] utilize the correlation of gaze behaviors and actions, modeling them jointly with a convolutional network. Lai *et al.* [33] encode global scene context into a single global token and explicitly model the global-local correlations in the visual embedding for gaze estimation. In contrast, egocentric gaze anticipation, which seeks to predict future gaze targets from past video frames, addresses an understudied dimension of modeling gaze. Zhang *et al.* [65] introduce this task and utilize a convolutional network and a discriminator to generate future video frames, which are further used to anticipate future gaze targets. They enhance their model by adding an additional branch for gaze forecasting [66]. All previous efforts on both egocentric gaze estimation and anticipation model gaze behavior from only the visual properties of the video stream, and do not consider the relationship between audio signals and gaze behavior. In this work, we introduce the first model that leverages both visual and audio signals for egocentric gaze anticipation.

Audio-Visual Saliency Prediction. Audio-visual saliency prediction is a well-studied problem in computer vision [9, 41, 48, 49, 51, 53]. Another related research topic is sound source localization [5, 20–23, 52] which localizes sound source in the image/video corresponding to a given audio stream. Here, we mainly discuss previous approaches for fusing audio and visual representations. Early CNN-based approaches adopt a late-fusion strategy [42, 57–60] for saliency prediction. Recently, new findings suggest audio-visual fusion at the intermediate features is a more effective way to leverage advantages of both modalities [1, 8, 55, 63] for saliency prediction. Jain *et al.* [27] investigate two fusion methods at the middle level which achieve new state of the art on multiple datasets. Yao *et al.* [64] propose to incorporate the audio signal at multiple decoder layers by using an inner-product operation. Similarly, Chang *et al.* [6] and Xiong *et al.* [62] merge audio features into visual features at multiple levels of the visual encoder. Notably, transformer-based fusion methods have not been applied in the audio-visual saliency prediction problem. Moreover, comparing to these prior works, the complex camera mo-

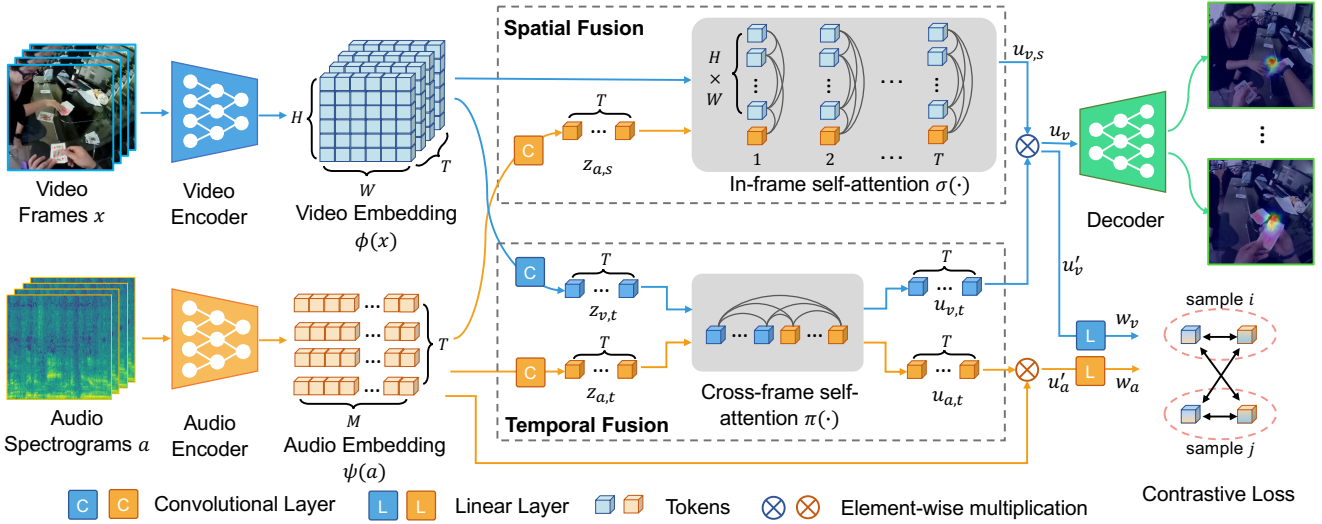


Figure 2. Overview of the proposed model. The video embeddings $\phi(x)$ and audio embeddings $\psi(a)$ are obtained by two transformer-based encoders. We then model the correlations of visual and audio embeddings using two separate branches – (1) spatial fusion, which learns the spatial co-occurrence of audio signals and visual objects in each frame, and (2) temporal fusion, which captures the temporal correlations and possible gaze movement. A contrastive loss is adopted to facilitate audio-visual representation learning. We input the fused embeddings into a decoder for final gaze anticipation results.

tion, drastic gaze movement, and the forecasting setting of egocentric gaze anticipation problem require a model that can explicitly understand how audio signals correlate with visual signals in both spatial and temporal dimensions. We implement the audio-visual fusion strategy widely used by prior work in our backbone. Experiment results in Sec. 4.2.2 demonstrate that the spatial-temporal separable fusion mechanism in our model is a more effective strategy.

Contrastive Audio-Visual Representation Learning. Our work draws from a rich literature on leveraging contrastive learning to learn audiovisual feature representations [2–4, 16, 18, 32, 39, 40, 43–46]. These works learn correspondences between audio and visual signals in an self-supervised manner, constructing positive pairs from matching video frames and audio segments, and negative pairs from all other pairwise combinations. We employ a similar contrastive loss to learn correspondences between co-occurring audio and visual features. However, while prior methods calculate contrastive loss on the raw embedding from each modality, we propose to apply contrastive loss on re-weighted audio and visual representations from our proposed spatial and temporal fusion mechanism.

3. Method

The egocentric gaze anticipation problem is illustrated in Fig. 1. Given an egocentric video and audio from time $t - \tau_a$ to t , the goal is to predict the future gaze from t to $t + \tau_a$ seconds. We denote the input video and audio as x and a , respectively, and model the gaze fixation as a probabilistic distribution on a 2D image plane (following [33, 35]).

Notably, video and audio signals have correlations in both spatial and temporal dimensions: Spatially, the audio signal will have the strongest correlation with the regions of the video frames that correspond to the sound source. Temporally, in egocentric video, audio stimuli in the scene drive the wearer’s head movement and how they orient the camera’s field of view. Our key insight is thus to separate the connection between audio and visual signals into spatial and temporal correlations.

Fig. 2 demonstrates the overview of our model. We exploit the transformer-based backbone encoders $\phi(x)$ and $\psi(a)$ to extract the representations of the video frames x and audio signals a . We then employ a Contrastive Spatial-Temporal Separable (CSTS) audio-visual fusion approach. Specifically, a spatial fusion module captures the correlation between audio embeddings and spatial appearance-based features; a temporal fusion module captures the temporal correlation between the visual and audio embeddings; and a contrastive loss is applied on fused audio-visual embeddings to facilitate the representation learning. Finally, spatially and temporally fused audio-visual features are merged and fed into a decoder for future gaze anticipation.

3.1. Audio and Visual Feature Embedding

Visual Feature Embedding. We adopt the multi-scale vision transformer (MViT) architecture [12] as the video encoder $\phi(x)$. $\phi(x)$ splits the 3D video tensor input into multiple non-overlapping patches, and thereby extracts $T \times H \times W$ visual tokens with feature dimension D from x .

Audio Feature Embedding. We follow [31] to adopt a

sliding window approach for audio signal preprocessing. Specifically, for a video frame at time step t_i , the corresponding audio segment has a range of $[t_i - \frac{1}{2}\Delta t_w, t_i + \frac{1}{2}\Delta t_w]$. We then use STFT to convert all audio segments into log-spectrograms and feed the processed audio segments into a transformer-based audio encoder $\psi(a)$. Since the audio stream has more sparse information than video stream, we follow [10, 14] to adopt a light-weighted transformer architecture for the audio encoder $\psi(a)$. In this way, $\psi(a)$ extracts $T \times M$ tokens with feature dimension D from the audio inputs a .

3.2. Spatial-Temporal Separable Fusion

Spatial Audio-Visual Fusion. The Spatial Fusion branch identifies correlations between the audio signal corresponding to a video frame and its visual content in space. We first use convolutional operations to generate the spatial fusion audio embedding $z_{a,s}$ with dimensions $T \times 1 \times D$ from the audio embedding $\psi(a)$. This allows the model to extract a holistic audio embedding within each sliding window. We then input the visual embedding $\phi(x)$ and pooled audio embedding $z_{a,s}$ into an in-frame self-attention layer σ . In this layer, we masked out all cross-frame connections and only calculate the correlations among visual tokens within each frame and the corresponding single audio token.

Therefore, the input to the spatial fusion consists of T groups of visual tokens, and T single audio embeddings. Formally, we have:

$$\phi(x) = [\phi(x)^{(1)}, \dots, \phi(x)^{(T)}], \quad (1)$$

$$z_{a,s} = [z_{a,s}^{(1)}, \dots, z_{a,s}^{(T)}], \quad (2)$$

where $\phi(x)^{(i)} \in \mathbb{R}^{1 \times N \times D}$, $z_{a,s}^{(i)} \in \mathbb{R}^{1 \times 1 \times D}$ with $i \in \{1, \dots, T\}$, and $N = H \times W$. Hence, the input from each time step is denoted as:

$$z_s^{(i)} = [\phi^{(i)}(x), z_{a,s}^{(i)}] \in \mathbb{R}^{1 \times (N+1) \times D} \quad (3)$$

The in-frame self-attention operation for time step i can be written as:

$$\sigma(z_s^{(i)}) = \text{Softmax} \left(\mathbf{Q}_s^{(i)} \mathbf{K}_s^{(i)T} / \sqrt{D} \right) \mathbf{V}_s^{(i)} \in \mathbb{R}^{1 \times (N+1) \times D}, \quad (4)$$

where $\mathbf{Q}_s^{(i)}$, $\mathbf{K}_s^{(i)}$, $\mathbf{V}_s^{(i)}$ refer to query, key, and value of the spatial self-attention at time step i , respectively. We apply Eq. 4 independently for each time step i and have the following overall in-frame self-attention:

$$\sigma(z_s) = [\sigma(z_s^{(1)}), \dots, \sigma(z_s^{(T)})] \in \mathbb{R}^{T \times (N+1) \times D}. \quad (5)$$

In practice, we input all tokens to the in-frame self-attention layer simultaneously, mask out cross-frame correlations and calculate Eq. 4 in one shot to speed up training. We further add two linear layers after the self-attention outputs $\sigma(z_s)$,

following the standard self-attention layer. The output of the spatial module is finally denoted as $u_s \in \mathbb{R}^{T \times (N+1) \times D}$.

Temporal Audio-Visual Fusion. The Temporal Fusion branch models relationships between audio and visual content across time. We apply two convolutional layers to integrate the embedding from each modality at each time step into a single token. The resulting visual and audio tokens are denoted as $z_{v,t} \in \mathbb{R}^{T \times 1 \times D}$ and $z_{a,t} \in \mathbb{R}^{T \times 1 \times D}$, respectively. Then we feed $z_t = [z_{v,t}, z_{a,t}] \in \mathbb{R}^{2T \times 1 \times D}$ into a cross-frame self-attention layer π :

$$\pi(z_t) = \text{Softmax} \left(\mathbf{Q}_t \mathbf{K}_t^T / \sqrt{D} \right) \mathbf{V}_t \in \mathbb{R}^{2T \times 1 \times D}, \quad (6)$$

where \mathbf{Q}_t , \mathbf{K}_t , \mathbf{V}_t are query, key and value matrices with dimension $2T \times 1 \times D$. Similar to the spatial fusion, two additional linear layers are added after $\pi(z_t)$ and result in the final temporal fusion output $u_t \in \mathbb{R}^{2T \times 1 \times D}$.

Merging of Two Fusion Modules. After obtaining audio-visual representations from the two fusion modules, we merge the two branches by reweighting the output from spatial fusion with the temporal weights from temporal fusion in each channel to obtain a new representation for each modality that has been refined by multimodal spatial and temporal correlation. Specifically, we break down the output from spatial fusion $u_s \in \mathbb{R}^{T \times (N+1) \times D}$ into $u_{v,s} \in \mathbb{R}^{T \times N \times D}$ and $u_{a,s} \in \mathbb{R}^{T \times 1 \times D}$, and the output from temporal fusion $u_t \in \mathbb{R}^{2T \times 1 \times D}$ into $u_{v,t} \in \mathbb{R}^{T \times 1 \times D}$ and $u_{a,t} \in \mathbb{R}^{T \times 1 \times D}$. The reweighted visual representation is formulated as

$$u_v = u_{v,s} \otimes u_{v,t} \in \mathbb{R}^{T \times N \times D}, \quad (7)$$

where \otimes denotes element-wise multiplication with broadcast mechanism. u_v is then fed into a decoder to generate final prediction for future gaze target. We follow [33] to add skip connections from the video encoder to the decoder and optimize the network with a KL-Divergence loss \mathcal{L}_{kld} .

3.3. Contrastive Learning for Audio-Visual Fusion

In addition to using KL-Divergence loss to supervise gaze anticipation, we propose to leverage the intrinsic alignment of visual and audio modalities to learn a more robust audio-visual representation by using a contrastive learning scheme. Multi-modal contrastive loss has been proved to be effective in self-supervised learning [2, 3]. Rather than calculating the contrastive loss directly on embedded features, we propose to use the reweighted video and audio representations from the spatial and temporal fusion modules. In our experiments, we show this is a more effective representation learning method for egocentric gaze anticipation.

To this end, we reweight the raw audio embedding $\psi(a) \in \mathbb{R}^{T \times M \times D}$ from the audio encoder by temporal weights $u_{a,t}$ from the temporal fusion module in a similar way to Eq. 7. We then get the reweighted audio feature as:

$$u_a = \psi(a) \otimes u_{a,t} \in \mathbb{R}^{T \times M \times D} \quad (8)$$

We don't use an additional learnable token to aggregate information from other tokens as prior works did [2, 3, 36]. We instead average all tokens of u_v and u_a respectively to obtain the single-vector representations $u'_v, u'_a \in \mathbb{R}^{1 \times D}$ and then map them to a common space using linear layers followed by L2-norm. It can be formulated as $w_v = \text{Norm}(f_1(u'_v))$ and $w_a = \text{Norm}(f_2(u'_a))$, where $f_1(\cdot), f_2(\cdot)$ are linear layers. The resulting visual vector and audio vector are denoted as $w_v, w_a \in \mathbb{R}^{1 \times D'}$, where D' is the new dimension of the common space. Within each mini-batch, corresponding audio and visual embeddings are considered as positive pairs, and all other pairwise combinations are considered as negative pairs. Following [36], we calculate video-to-audio loss and audio-to-video loss separately. The video-to-audio contrastive loss is defined as

$$\mathcal{L}_{cntr}^{v2a} = -\frac{1}{|\mathcal{B}|} \sum_{i=1}^{|\mathcal{B}|} \log \frac{\exp(w_v^{(i)T} w_a^{(i)}/\mathcal{T})}{\sum_{j \in \mathcal{B}} \exp(w_v^{(i)T} w_a^{(j)}/\mathcal{T})}, \quad (9)$$

where \mathcal{B} is the training batch $\mathcal{B} = \{1, 2, \dots, n\}$ and \mathcal{T} is the temperature factor. Superscripts (i) and (j) denote the i -th and j -th samples in the batch. The audio-to-video loss is defined in a symmetric way. Finally, the contrastive loss is defined as $\mathcal{L}_{cntr} = \mathcal{L}_{cntr}^{v2a} + \mathcal{L}_{cntr}^{a2v}$. \mathcal{L}_{kld} and \mathcal{L}_{cntr} are linearly combined with a parameter α for the final training loss, *i.e.* $\mathcal{L} = \mathcal{L}_{kld} + \alpha \mathcal{L}_{cntr}$.

3.4. Implementation Details

In our experiments, we set observation time τ_o as 3 seconds and anticipation time τ_a as 2 seconds. For video input, we sample 8 frames from the observable segment and resize to a spatial size of 256×256 . For audio input, following [31], we first resample the audio signal to 24kHz and set a time window with $\Delta t_w = 1.28s$ to crop the audio segment corresponding to each video frame. We then convert it to a log-spectrogram using a STFT with window size 10ms and hop length 5ms. The number of frequency bands is set as 256 resulting in a spectrogram matrix of size 256×256 . The output of the decoder is the gaze distribution on 8 frames uniformly sampled from the 2-second anticipation time. More details about model architecture and training hyper-parameters can be found in the supplementary.

4. Experiments

We first introduce the datasets and evaluation metrics used in our experiments. We then present detailed ablation studies to validate the contribution of each component in our method, and demonstrate the performance improvement over prior SOTA methods for gaze anticipation as well as gaze estimation models applied to the gaze anticipation

task. Finally, we visualize the predictions and weights of our model to provide qualitative insight into our method.

4.1. Experiment Setup

Datasets. We conduct experiments on two egocentric datasets¹ that contain aligned video and audio streams and gaze tracking data – Ego4D [17] and Aria [29]. The Ego4D eye-tracking subset is collected in social settings and totals 31 hours of egocentric videos from 80 participants. All videos have a fixed 30 fps frame rate and spatial resolution of 1088×1080 , and audio streams are recorded with a sampling rate of 44.1kHz. We use the train/test split released in [33] in our experiments, *i.e.*, 15310 video segments for training and the other 5202 video segments for testing.

The Aria dataset contains 143 egocentric videos (totaling 7.5 hours) collected with Project Aria glasses. It covers a variety of everyday activities including cooking, exercising and spending time with friends. All videos have a fixed 30 fps frame rate and spatial resolution of 1408×1408 . A sliding window is used to trim long videos into 5-second video segment with a stride of 2 seconds. We use 107 videos (10456 segments) for training and 36 videos (2901 segments) for testing. We will release our split to facilitate future studies in this direction.

Evaluation Metrics. As suggested in recent work on egocentric gaze estimation [33], AUC score can easily get saturated due to the long-tailed distribution of gaze on 2D video frames. Therefore, we follow [33, 35] to adopt F1 score, recall and precision as our evaluation metrics.

4.2. Experimental Results

4.2.1 Ablation Study

We first quantify the performance contribution of each key module from our proposed method. Specifically, we denote the model with only spatial fusion module as *S-fusion*, the model with only temporal fusion as *T-fusion*, the model uses our proposed spatial-temporal fusion module without the contrastive learning schema as *STS*. As demonstrated in Table 1, compared with models trained solely on RGB frames (Vision only), S-fusion and T-fusion boost the F1 score by +1.4% and +1.5% on Ego4D, and +1.1% and +1.1% on Aria. Moreover, the STS model further achieves a F1 score of 39.2% on Ego4D and 59.3% on Aria. These results suggest that both the spatial and the temporal correlation between video and audio signal play a vital role for egocentric gaze anticipation. Contrastive loss further improves F1 by +0.5% and +0.6% suggesting its notable contributions to audio-visual representative learning.

¹Note that another widely used gaze estimation benchmark EGTEA Gaze+ [35] did not release audio data and thus is not feasible for our study.

Methods	Ego4D			Aria		
	F1	Rec.	Prec.	F1	Rec.	Prec.
Vision only	37.2	54.1	28.3	57.5	62.4	53.3
S-fusion	38.6	54.1	30.1	58.6	67.1	52.0
T-fusion	38.7	53.8	30.1	58.6	65.9	52.8
STS	39.2	53.7	30.8	59.3	66.8	53.3
CSTS	39.7	53.3	31.6	59.9	66.8	54.3

Table 1. Ablations on each key component of our proposed model. The best results are highlighted with **boldface**. See Section 4.2.1 for further discussion.

Methods	Ego4D			Aria		
	F1	Rec.	Prec.	F1	Rec.	Prec.
Vision only	37.2	54.1	28.3	57.5	62.4	53.3
Concat.	38.1	53.6	29.5	58.0	66.8	51.2
Vanilla SA	38.5	53.3	30.1	58.0	67.2	51.1
Seq. ST	38.5	53.6	30.1	58.6	67.3	52.0
STS	39.2	53.7	30.8	59.3	66.8	53.3

Table 2. Analysis on proposed fusion strategies. The best results are highlighted with **boldface**. STS refers to the proposed spatial-temporal separable fusion method (without contrastive learning). See Section 4.2.2 for details.

4.2.2 Analysis on Fusion and Contrastive Learning

Directly feeding all visual and audio tokens into a fusion layer (*i.e.* joint fusion) is a widely used approach for audio-visual saliency prediction [6, 58, 62] and sound source localization [5, 7, 21, 47]. To show the superiority of the proposed spatial-temporal separable (STS) fusion approach, we provide additional analysis of three joint fusion strategies: (1) concatenating audio and visual embeddings along channel dimension (denoted as *Concat.*) as in [27, 31]; (2) feeding all embedded video and audio tokens together into a standard self-attention layer (denoted as *Vanilla SA*), which is inspired by [37, 62]; and (3) a variant of STS that connects the two fusion modules sequentially, *i.e.* feeding embeddings to the temporal fusion module first and then feeding its output to the spatial fusion module (denoted as *Seq. ST*). We further detail how our design differs from the above fusion strategies in the supplementary.

As shown in Table 2, *Concat.* and *Vanilla SA* has limited improvement over the vision-only baseline, suggesting that previous audio-visual fusion methods, which follow these strategies, are sub-optimal for our problem setting. In contrast, our proposed fusion strategy yields larger performance boost (+2.0% on Ego4D and +1.8% on Aria), even without using the contrastive loss (STS), which shows the benefits of our proposed spatial-temporal separable fusion mechanism. Additionally, our model also consistently surpasses its sequential variant (Seq. ST) by +0.7% on both datasets, further demonstrating the benefits of explicitly rea-

Methods	Ego4D			Aria		
	F1	Rec.	Prec.	F1	Rec.	Prec.
Vanilla SA	38.5	53.3	30.1	58.0	67.2	51.1
SA + Vanilla Contr	38.5	52.4	30.5	58.4	67.0	51.8
SA + Post Contr	38.9	54.4	30.3	58.8	66.4	52.8
STS	39.2	53.7	30.8	59.3	66.8	53.3
STS + Vanilla Contr	39.0	53.7	30.6	59.1	66.5	53.1
STS + Post Contr	39.7	53.3	31.6	59.9	66.8	54.3

Table 3. Analysis on proposed contrastive learning schema. The best results are highlighted with **boldface**. The highlighted row refers to the complete CSTS model. See Section 4.2.2 for details.

soning spatial and temporal correlation separately.

We also evaluate the benefits of our contrastive learning scheme in Table 3. Here, we consider another baseline (denoted as *Vanilla Contr*) that calculates the contrastive loss using raw video and audio embeddings (*i.e.* $\phi(x)$ and $\psi(a)$), as is typical in prior work [16, 18, 39, 56]. Our strategy of adding contrastive loss on fused features is denoted as *Post Contr*. *Vanilla Contr* makes only minor differences on *Vanilla SA* model and even slightly reduces performance when accompanied by our proposed STS mechanism. In contrast, our proposed Post Contr schema improves the performance of *Vanilla SA* by +0.4% and 0.8% and improves STS by +0.5% and +0.6% on the two datasets. These results further suggest that post-fusion contrastive learning is more robust for audio-visual representation learning. Additional experiments with different contrastive learning strategies are provided in the supplementary.

4.2.3 Comparison with State-of-the-art Methods

Most existing works on egocentric gaze modeling target egocentric gaze estimation rather than anticipation. In order to provide a thorough comparison, in addition to comparing against SOTA egocentric gaze anticipation models (DFG[65], DFG+[66]), we also adapt the recent SOTA egocentric gaze estimation model GLC[33] and all baselines from [33] (I3D-Res50 [61], MViT[12], GazeMLE[35] and AttnTrans[24]) to the anticipation task. Detailed results are summarized in Table 4.

Our method outperforms its direct competitor DFG+, which is the previous SOTA model for egocentric gaze anticipation, by +2.4% F1 on Ego4D and +2.3% F1 on Aria. Note that the original DFG and DFG+ used a less powerful backbone encoder, so for fair comparison, we reimplement their method using the same MViT backbone as our method. We also observe that methods originally designed for egocentric gaze estimation still work as strong baselines for the egocentric gaze anticipation task. Our proposed CSTS model also outperforms these methods, surpassing the recent SOTA for egocentric gaze estimation, GLC, by +1.9% F1 on Ego4D and +1.6% F1 on Aria.

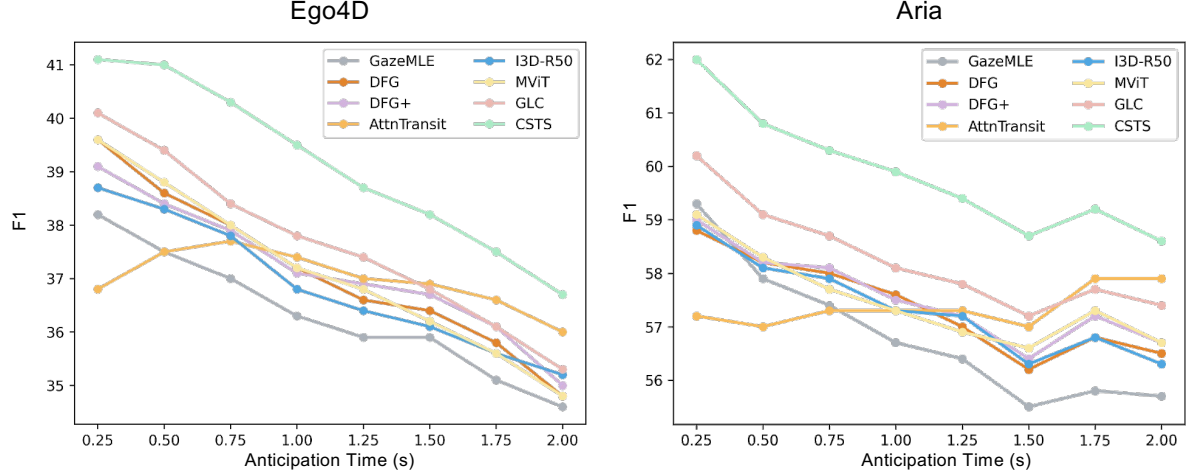


Figure 3. The performance of gaze anticipation in each frame. Our model consistently outperforms all prior methods by a notable margin.

Methods	Ego4D			Aria		
	F1	Rec.	Prec.	F1	Rec.	Prec.
Center Prior	13.6	9.4	24.2	24.9	17.3	44.4
GazeMLE [35]	36.3	52.5	27.8	56.8	64.1	51.0
AttnTrans [24]	37.0	55.0	27.9	57.4	65.5	51.0
I3D-R50 [13]	36.9	52.1	28.6	57.4	63.6	52.2
MViT [12]	37.2	54.1	28.3	57.5	62.4	53.3
GLC [33]	37.8	52.9	29.4	58.3	65.4	52.6
DFG [65]	37.2	53.2	28.6	57.4	63.6	52.3
DFG+ [66]	37.3	52.3	29.0	57.6	65.5	51.3
CSTS	39.7	53.3	31.6	59.9	66.8	54.3

Table 4. Comparison with previous state-of-the-art models on egocentric gaze anticipation. We also adapt previous egocentric gaze estimation approaches to the anticipation setting for a more thorough comparison. The best results are highlighted with **boldface**. See Section 4.2.3 for further discussion.

In addition, we evaluate gaze anticipation on each anticipation time step independently and compare with previous methods in Fig. 3. Unsurprisingly, the anticipation problem becomes more challenging as the anticipation time step increases farther into the future. Our CSTS method consistently outperforms all baselines at all future time steps. We also note that our model produces new SOTA results on egocentric gaze estimation, demonstrating the generalizability and robustness of our approach across gaze modeling tasks. We include these results in the supplementary.

4.2.4 Visualization of Predictions

We visually showcase the anticipation results of CSTS and the baselines in Fig. 5. We can see that GazeMLE [35] and AttnTransit [24] produce more ambiguity in prediction heatmaps. Other methods fail to anticipate the true gaze

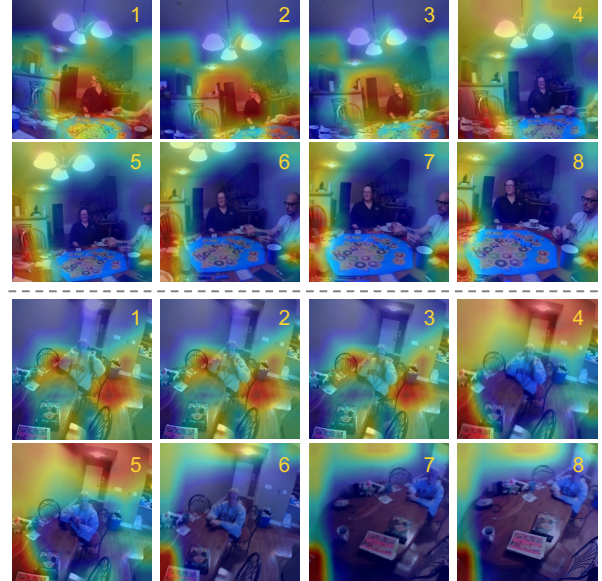


Figure 4. Visualization of the spatial correlation weights. All video frames are sorted in a chronological order indexed by the numbers on the top-right corner.

target, and are likely misled by other salient objects. Our CSTS approach produces the best gaze anticipation results among all methods. We attribute this improvement to our novel model design that effectively leverages both audio and visual cues for forecasting the gaze targets.

4.2.5 Visualization of Learned Correlations

We provide further insight on our model by visualizing the audio-visual correlation from the spatial fusion module. For each time step t , we calculate the correlation of each visual token with the single audio token and map it back to the input frames. The correlation heatmaps are shown in Fig. 4.

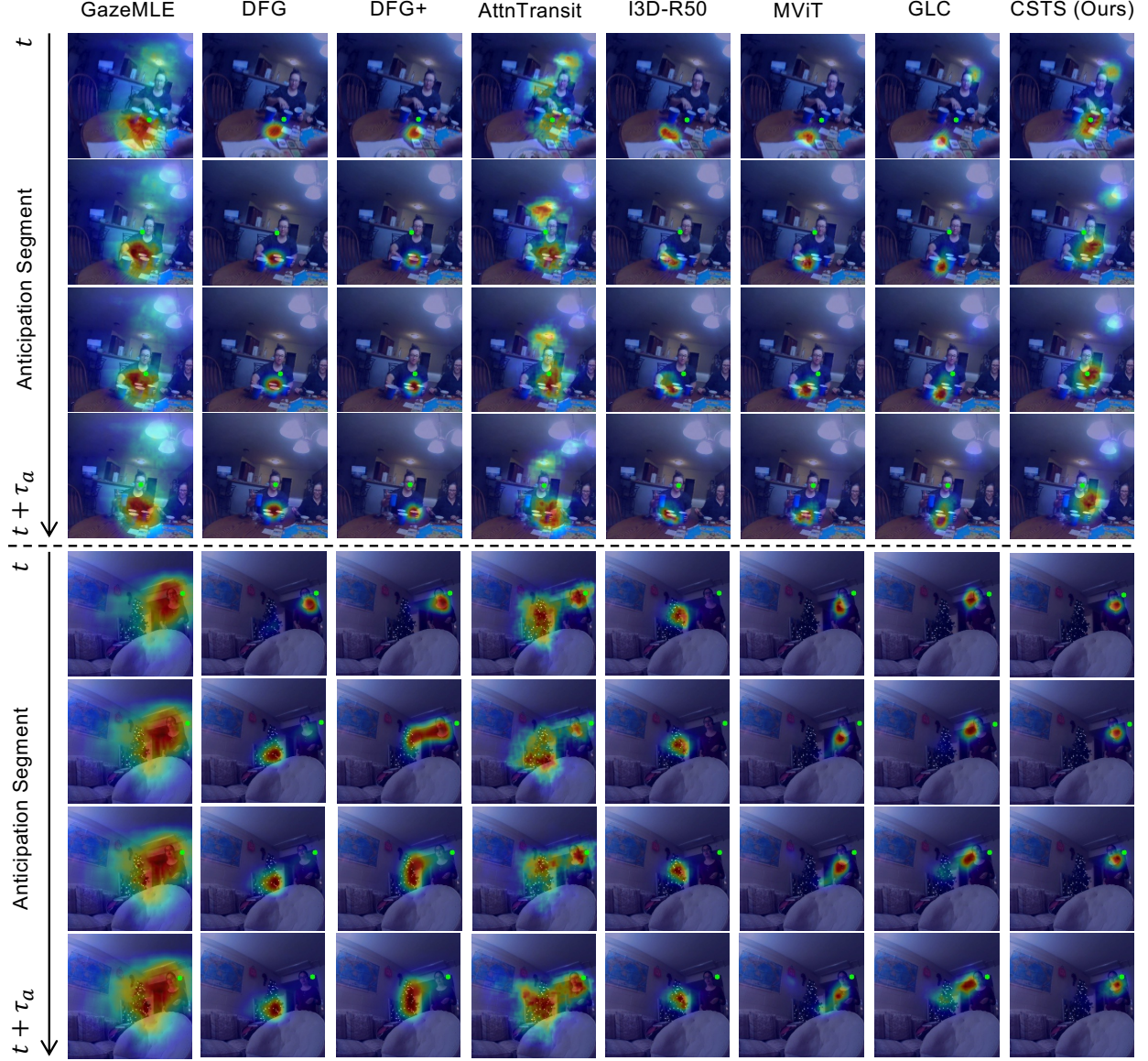


Figure 5. Egocentric gaze anticipation results from our model and other baselines. We show the results of four future time steps uniformly sampled from the anticipation segments. **Green dots** indicate the ground truth gaze location.

In the first example, the speaker in the middle speaks, then turns her head around to talk with a social partner in the background (*e.g.* frame 1-3). We observe that our model captures that the audio signal has the highest correlation with spatial region of the speaker while she is speaking. Then, when she stops talking and turns her head back, the correlation is highest in the background regions, indicating the potential location of her social partner. The second example illustrates a similar phenomenon; the model captures the speaker at the beginning when she is talking, then attend to background locations when she stops. These examples suggest our model has the capability to model the audio-visual correlations in spatial dimension to learn a robust audio-visual representation.

bust audio-visual representation.

5. Conclusion

In this paper, we propose a novel contrastive spatial-temporal separable fusion approach (CSTS) for egocentric gaze anticipation. Our key contribution is to break down the fusion of the audio and visual modalities into a separate spatial fusion module for learning the spatial co-occurrence of salient visual features and audio signals, and a temporal fusion module for modeling the audio-visual correlations across different time steps. We further adopt a contrastive loss on the reweighted audio-visual representations

from the fusion modules to facilitate multimodal representation learning. We demonstrate the benefits of our proposed model design on two egocentric video datasets: Ego4D and Aria. Our work is a key step for probing into human cognitive process with computational models, and provides important insights into multimodal representation learning, visual forecasting, and egocentric video understanding.

References

- [1] Ritvik Agrawal, Shreyank Jyoti, Rohit Girmaji, Sarath Sivaprasad, and Vineet Gandhi. Does audio help in deep audio-visual saliency prediction models? In *Proceedings of the 2022 International Conference on Multimodal Interaction*, pages 48–56, 2022. 2
- [2] Hassan Akbari, Liangzhe Yuan, Rui Qian, Wei-Hong Chuang, Shih-Fu Chang, Yin Cui, and Boqing Gong. Vatt: Transformers for multimodal self-supervised learning from raw video, audio and text. *Advances in Neural Information Processing Systems*, 34:24206–24221, 2021. 2, 3, 4, 5
- [3] Jean-Baptiste Alayrac, Adria Recasens, Rosalia Schneider, Relja Arandjelović, Jason Ramapuram, Jeffrey De Fauw, Lucas Smaira, Sander Dieleman, and Andrew Zisserman. Self-supervised multimodal versatile networks. *Advances in Neural Information Processing Systems*, 33:25–37, 2020. 4, 5
- [4] Relja Arandjelovic and Andrew Zisserman. Look, listen and learn. In *Proceedings of the IEEE international conference on computer vision*, pages 609–617, 2017. 3
- [5] Relja Arandjelovic and Andrew Zisserman. Objects that sound. In *Proceedings of the European conference on computer vision (ECCV)*, pages 435–451, 2018. 2, 6
- [6] Qinyao Chang and Shiping Zhu. Temporal-spatial feature pyramid for video saliency detection. *Cognitive Computation*, 2021. 2, 6
- [7] Honglie Chen, Weidi Xie, Triantafyllos Afouras, Arsha Nagrani, Andrea Vedaldi, and Andrew Zisserman. Localizing visual sounds the hard way. In *Proceedings of the IEEE/CVF Conference on Computer Vision and Pattern Recognition*, pages 16867–16876, 2021. 2, 6
- [8] Shuaiyang Cheng, Xing Gao, Liang Song, and Jianbing Xiahou. Audio-visual saliency network with audio attention module. In *2021 2nd International Conference on Artificial Intelligence and Information Systems*, pages 1–5, 2021. 2
- [9] Antoine Coutrot and Nathalie Guyader. Multimodal saliency models for videos. *From Human Attention to Computational Attention: A Multidisciplinary Approach*, pages 291–304, 2016. 2
- [10] Alexey Dosovitskiy, Lucas Beyer, Alexander Kolesnikov, Dirk Weissenborn, Xiaohua Zhai, Thomas Unterthiner, Mostafa Dehghani, Matthias Minderer, Georg Heigold, Sylvain Gelly, et al. An image is worth 16x16 words: Transformers for image recognition at scale. *International Conference on Learning Representations*, 2020. 4
- [11] Haoqi Fan, Yanghao Li, Bo Xiong, Wan-Yen Lo, and Christoph Feichtenhofer. Pyslowfast. <https://github.com/facebookresearch/slowfast>, 2020. 14
- [12] Haoqi Fan, Bo Xiong, Karttikeya Mangalam, Yanghao Li, Zhicheng Yan, Jitendra Malik, and Christoph Feichtenhofer. Multiscale vision transformers. In *Proceedings of the IEEE/CVF International Conference on Computer Vision*, pages 6824–6835, 2021. 3, 6, 7, 12, 13
- [13] Christoph Feichtenhofer, Haoqi Fan, Jitendra Malik, and Kaiming He. Slowfast networks for video recognition. In *Proceedings of the IEEE/CVF international conference on computer vision*, pages 6202–6211, 2019. 7, 13
- [14] Ruohan Gao, Tae-Hyun Oh, Kristen Grauman, and Lorenzo Torresani. Listen to look: Action recognition by previewing audio. In *Proceedings of the IEEE/CVF Conference on Computer Vision and Pattern Recognition*, pages 10457–10467, 2020. 4, 12
- [15] Xavier Glorot and Yoshua Bengio. Understanding the difficulty of training deep feedforward neural networks. In *Proceedings of the thirteenth international conference on artificial intelligence and statistics*, pages 249–256. JMLR Workshop and Conference Proceedings, 2010. 12
- [16] Yuan Gong, Andrew Rouditchenko, Alexander H Liu, David Harwath, Leonid Karlinsky, Hilde Kuehne, and James Glass. Contrastive audio-visual masked autoencoder. *International Conference on Learning Representations*, 2022. 3, 6
- [17] Kristen Grauman, Andrew Westbury, Eugene Byrne, Zachary Chavis, Antonino Furnari, Rohit Girdhar, Jackson Hamburger, Hao Jiang, Miao Liu, Xingyu Liu, et al. Ego4d: Around the world in 3,000 hours of egocentric video. In *Proceedings of the IEEE/CVF Conference on Computer Vision and Pattern Recognition*, pages 18995–19012, 2022. 2, 5, 13
- [18] Sumanth Gurram, Andy Fang, David Chan, and John Canny. Lava: Language audio vision alignment for contrastive video pre-training. *arXiv preprint arXiv:2207.08024*, 2022. 3, 6
- [19] Mary Hayhoe and Dana Ballard. Eye movements in natural behavior. *Trends in cognitive sciences*, 9(4):188–194, 2005. 1
- [20] Di Hu, Feiping Nie, and Xuelong Li. Deep multimodal clustering for unsupervised audiovisual learning. In *Proceedings of the IEEE/CVF Conference on Computer Vision and Pattern Recognition*, pages 9248–9257, 2019. 2
- [21] Di Hu, Rui Qian, Minyue Jiang, Xiao Tan, Shilei Wen, Errui Ding, Weiyao Lin, and Dejing Dou. Discriminative sounding objects localization via self-supervised audiovisual matching. *Advances in Neural Information Processing Systems*, 33:10077–10087, 2020. 2, 6
- [22] Xixi Hu, Ziyang Chen, and Andrew Owens. Mix and localize: Localizing sound sources in mixtures. In *Proceedings of the IEEE/CVF Conference on Computer Vision and Pattern Recognition*, pages 10483–10492, 2022.
- [23] Chao Huang, Yapeng Tian, Anurag Kumar, and Chenliang Xu. Egocentric audio-visual object localization. In *Proceedings of the IEEE/CVF Conference on Computer Vision and Pattern Recognition*, pages 22910–22921, 2023. 2
- [24] Yifei Huang, Minjie Cai, Zhenqiang Li, and Yoichi Sato. Predicting gaze in egocentric video by learning task-dependent attention transition. In *Proceedings of the European conference on computer vision (ECCV)*, pages 754–769, 2018. 2, 6, 7, 13

[25] Yifei Huang, Minjie Cai, Zhenqiang Li, Feng Lu, and Yoichi Sato. Mutual context network for jointly estimating egocentric gaze and action. *IEEE Transactions on Image Processing*, 29:7795–7806, 2020. 2

[26] Yifei Huang, Minjie Cai, and Yoichi Sato. An ego-vision system for discovering human joint attention. *IEEE Transactions on Human-Machine Systems*, 50(4):306–316, 2020. 2

[27] Samyak Jain, Pradeep Yarlagadda, Shreyank Jyoti, Shyamgopal Karthik, Ramanathan Subramanian, and Vineet Gandhi. Vinet: Pushing the limits of visual modality for audio-visual saliency prediction. In *2021 IEEE/RSJ International Conference on Intelligent Robots and Systems (IROS)*, pages 3520–3527. IEEE, 2021. 2, 6

[28] Wenqi Jia, Miao Liu, and James M Rehg. Generative adversarial network for future hand segmentation from egocentric video. In *Computer Vision–ECCV 2022: 17th European Conference, Tel Aviv, Israel, October 23–27, 2022, Proceedings, Part XIII*, pages 639–656. Springer, 2022. 13

[29] Selcuk Karakas, Pierre Moulon, Wenqi Zhang, Nan Yang, Julian Straub, Lingni Ma, Zhaoyang Lv, Elizabeth Argall, Georges Berenger, Tanner Schmidt, Kiran Somasundaram, Vijay Baiyya, Philippe Bouteffroy, Geof Sawaya, Yang Lou, Eric Huang, Tianwei Shen, David Caruso, Bilal Souti, Chris Sweeney, Jeff Meissner, Edward Miller, and Richard Newcombe. Aria data tools. https://github.com/facebookresearch/aria_data_tools, 2022. 2, 5, 13

[30] Will Kay, Joao Carreira, Karen Simonyan, Brian Zhang, Chloe Hillier, Sudheendra Vijayanarasimhan, Fabio Viola, Tim Green, Trevor Back, Paul Natsev, et al. The kinetics human action video dataset. *arXiv preprint arXiv:1705.06950*, 2017. 12

[31] Evangelos Kazakos, Arsha Nagrani, Andrew Zisserman, and Dima Damen. Epic-fusion: Audio-visual temporal binding for egocentric action recognition. In *Proceedings of the IEEE/CVF International Conference on Computer Vision*, pages 5492–5501, 2019. 3, 5, 6

[32] Bruno Korbar, Du Tran, and Lorenzo Torresani. Cooperative learning of audio and video models from self-supervised synchronization. *Advances in Neural Information Processing Systems*, 31, 2018. 3

[33] Bolin Lai, Miao Liu, Fiona Ryan, and James Rehg. In the eye of transformer: Global-local correlation for egocentric gaze estimation. *British Machine Vision Conference*, 2022. 2, 3, 4, 5, 6, 7, 12, 13

[34] Yin Li, Alireza Fathi, and James M Rehg. Learning to predict gaze in egocentric video. In *Proceedings of the IEEE international conference on computer vision*, pages 3216–3223, 2013.

[35] Yin Li, Miao Liu, and Jame Rehg. In the eye of the beholder: Gaze and actions in first person video. *IEEE Transactions on Pattern Analysis and Machine Intelligence*, 2021. 2, 3, 5, 6, 7, 12, 13

[36] Kevin Qinghong Lin, Alex Jinpeng Wang, Mattia Soldan, Michael Wray, Rui Yan, Eric Zhongcong Xu, Difei Gao, Rongcheng Tu, Wenzhe Zhao, Weijie Kong, et al. Egocentric video-language pretraining. *Advances in Neural Information Processing Systems*, 2022. 5, 12

[37] Yan-Bo Lin, Yi-Lin Sung, Jie Lei, Mohit Bansal, and Gedas Bertasius. Vision transformers are parameter-efficient audio-visual learners. *Proceedings of the IEEE Conference on Computer Vision and Pattern Recognition*, 2023. 6

[38] Ilya Loshchilov and Frank Hutter. Decoupled weight decay regularization. *arXiv preprint arXiv:1711.05101*, 2017. 12

[39] Shuang Ma, Zhaoyang Zeng, Daniel McDuff, and Yale Song. Active contrastive learning of audio-visual video representations. *International Conference on Learning Representations*, 2020. 3, 6

[40] Shuang Ma, Zhaoyang Zeng, Daniel McDuff, and Yale Song. Contrastive learning of global-local video representations. *arXiv preprint arXiv:2104.05418*, 2021. 3

[41] Xiongkuo Min, Guangtao Zhai, Ke Gu, and Xiaokang Yang. Fixation prediction through multimodal analysis. *ACM Transactions on Multimedia Computing, Communications, and Applications (TOMM)*, 13(1):1–23, 2016. 2

[42] Xiongkuo Min, Guangtao Zhai, Jiantao Zhou, Xiao-Ping Zhang, Xiaokang Yang, and Xinpeng Guan. A multimodal saliency model for videos with high audio-visual correspondence. *IEEE Transactions on Image Processing*, 29:3805–3819, 2020. 2

[43] Pedro Morgado, Yi Li, and Nuno Vasconcelos. Learning representations from audio-visual spatial alignment. *Advances in Neural Information Processing Systems*, 33:4733–4744, 2020. 3

[44] Pedro Morgado, Ishan Misra, and Nuno Vasconcelos. Robust audio-visual instance discrimination. In *Proceedings of the IEEE/CVF Conference on Computer Vision and Pattern Recognition*, pages 12934–12945, 2021.

[45] Pedro Morgado, Nuno Vasconcelos, and Ishan Misra. Audio-visual instance discrimination with cross-modal agreement. In *Proceedings of the IEEE/CVF Conference on Computer Vision and Pattern Recognition*, pages 12475–12486, 2021.

[46] Mandela Patrick, Yuki Asano, Polina Kuznetsova, Ruth Fong, Joao F Henriques, Geoffrey Zweig, and Andrea Vedaldi. Multi-modal self-supervision from generalized data transformations. *arXiv preprint*, 2020. 3

[47] Rui Qian, Di Hu, Heinrich Dinkel, Mengyue Wu, Ning Xu, and Weiyao Lin. Multiple sound sources localization from coarse to fine. In *Computer Vision–ECCV 2020: 16th European Conference, Glasgow, UK, August 23–28, 2020, Proceedings, Part XX 16*, pages 292–308. Springer, 2020. 2, 6

[48] Rémi Ratajczak, Denis Pellerin, Quentin Labourey, and Catherine Garbay. A fast audiovisual attention model for human detection and localization on a companion robot. In *VISUAL 2016-The First International Conference on Applications and Systems of Visual Paradigms (VISUAL 2016)*, 2016. 2

[49] Jonas Ruesch, Manuel Lopes, Alexandre Bernardino, Jonas Hornstein, José Santos-Victor, and Rolf Pfeifer. Multimodal saliency-based bottom-up attention a framework for the humanoid robot icub. In *2008 IEEE International Conference on Robotics and Automation*, pages 962–967. IEEE, 2008. 2

[50] KP Schaefer, KJ Süss, and E Fiebig. Acoustic-induced eye movements. *Annals of the New York Academy of Sciences*, 374:674–688, 1981. 1

[51] Boris Schauerte, Benjamin Kühn, Kristian Kroschel, and Rainer Stiefelhagen. Multimodal saliency-based attention for object-based scene analysis. In *2011 IEEE/RSJ International Conference on Intelligent Robots and Systems*, pages 1173–1179. IEEE, 2011. 2

[52] Arda Senocak, Tae-Hyun Oh, Junsik Kim, Ming-Hsuan Yang, and In So Kweon. Learning to localize sound source in visual scenes. In *Proceedings of the IEEE Conference on Computer Vision and Pattern Recognition*, pages 4358–4366, 2018. 2

[53] Naty Sidaty, Mohamed-Chaker Larabi, and Abdelhakim Saadane. Toward an audiovisual attention model for multimodal video content. *Neurocomputing*, 259:94–111, 2017. 2

[54] Hyun Soo Park and Jianbo Shi. Social saliency prediction. In *Proceedings of the IEEE Conference on Computer Vision and Pattern Recognition*, pages 4777–4785, 2015. 2

[55] Hamed R Tavakoli, Ali Borji, Esa Rahtu, and Juho Kannala. Dave: A deep audio-visual embedding for dynamic saliency prediction. *arXiv preprint arXiv:1905.10693*, 2019. 2

[56] Yapeng Tian, Jing Shi, Bochen Li, Zhiyao Duan, and Chenliang Xu. Audio-visual event localization in unconstrained videos. In *Proceedings of the European Conference on Computer Vision (ECCV)*, 2018. 6

[57] Antigoni Tsiami, Petros Koutras, Athanasios Katsamanis, Argyro Vatakis, and Petros Maragos. A behaviorally inspired fusion approach for computational audiovisual saliency modeling. *Signal Processing: Image Communication*, 76: 186–200, 2019. 2

[58] Antigoni Tsiami, Petros Koutras, and Petros Maragos. Stavis: Spatio-temporal audiovisual saliency network. In *Proceedings of the IEEE/CVF Conference on Computer Vision and Pattern Recognition*, pages 4766–4776, 2020. 2, 6

[59] Guotao Wang, Chenglizhao Chen, Deng-Ping Fan, Aimin Hao, and Hong Qin. From semantic categories to fixations: A novel weakly-supervised visual-auditory saliency detection approach. In *Proceedings of the IEEE/CVF conference on computer vision and pattern recognition*, pages 15119–15128, 2021.

[60] Guotao Wang, Chenglizhao Chen, Deng-Ping Fan, Aimin Hao, and Hong Qin. Weakly supervised visual-auditory fixation prediction with multigranularity perception. *arXiv preprint arXiv:2112.13697*, 2021. 2

[61] Xiaolong Wang, Ross Girshick, Abhinav Gupta, and Kaiming He. Non-local neural networks. In *Proceedings of the IEEE conference on computer vision and pattern recognition*, pages 7794–7803, 2018. 6

[62] Junwen Xiong, Ganglai Wang, Peng Zhang, Wei Huang, Yufei Zha, and Guangtao Zhai. Casp-net: Rethinking video saliency prediction from an audio-visual consistency perceptual perspective. In *Proceedings of the IEEE/CVF Conference on Computer Vision and Pattern Recognition*, pages 6441–6450, 2023. 2, 6

[63] Qin Yang, Yuqi Li, Chenglin Li, Hao Wang, Sa Yan, Li Wei, Wenrui Dai, Junni Zou, Hongkai Xiong, and Pascal Frossard. Svcg-ava: 360-degree video saliency prediction with spherical vector-based graph convolution and audio-visual attention. *IEEE Transactions on Multimedia*, 2023. 2

[64] Shunyu Yao, Xiongkuo Min, and Guangtao Zhai. Deep audio-visual fusion neural network for saliency estimation. In *2021 IEEE International Conference on Image Processing (ICIP)*, pages 1604–1608. IEEE, 2021. 2

[65] Mengmi Zhang, Keng Teck Ma, Joo Hwee Lim, Qi Zhao, and Jiashi Feng. Deep future gaze: Gaze anticipation on egocentric videos using adversarial networks. In *Proceedings of the IEEE conference on computer vision and pattern recognition*, pages 4372–4381, 2017. 2, 6, 7

[66] Mengmi Zhang, Keng Teck Ma, Joo Hwee Lim, Qi Zhao, and Jiashi Feng. Anticipating where people will look using adversarial networks. *IEEE transactions on pattern analysis and machine intelligence*, 41(8):1783–1796, 2018. 2, 6, 7

Listen to Look into the Future: Audio-Visual Egocentric Gaze Anticipation

Supplementary Material

This is the supplementary material for the paper titled "Listen to Look into the Future: Audio-Visual Egocentric Gaze Anticipation". We organize the content as follows:

- **A** – Implementation Details
- **B** – Details of Baseline Fusion Strategies
- **C** – Experiments on Contrastive Learning
- **D** – Results on Egocentric Gaze Estimation
- **E** – Additional Visualization
- **F** – Limitation and Future Work
- **G** – Code and License

A. Implementation Details

Architecture. Inspired by [14], we use a light-weight audio encoder composed of four self-attention blocks from MViT [12]. The model architecture is further detailed in Table 7. We initialize the video encoder with Kinetics-400 pretraining [30] and initialize the audio encoder using Xavier initialization [15]. The resulting video embeddings $\phi(x)$ have a dimension of $T = 4, H = 8, W = 8, D = 768$, and the resulting audio embeddings $\psi(a)$ have a dimension of $T = 4, M = 64, D = 768$. We follow [36] to map audio-visual representation vectors to dimension $D' = 256$ for the contrastive loss. The output from the decoder is a downsampled heatmap which is upsampled to match the input size using trilinear interpolation. Following [33], we add intermediate features from each video encoder block to the corresponding decoder block output via skip connections to compensate for the loss of low-level textures.

Training. We set both temperature factor \mathcal{T} of contrastive loss and re-weight parameter α as 0.05. Follow [33, 35], we use a Gaussian distribution with kernel size of 19 centered on the gaze location in each frame as the ground truth gaze heatmap during training. The model is trained with AdamW [38] optimization for 15 epochs. The momentum and weight decay are set as 0.9 and 0.05. The initial learning rate is 10^{-4} which decreases with the cosine learning rate decay strategy. The model is trained with a batch size of 8 across 4 GPUs.

B. Details of Baseline Fusion Strategies

We compare with multiple different audio-visual fusion strategies in main paper Table 2. The details of each baseline are listed as follows:

Concat. We reshape the audio embedding $\psi(a) \in \mathbb{R}^{T \times H \times W \times D}$ to the same dimension as the video embedding $\phi(x) \in \mathbb{R}^{T \times H \times W \times D}$ and concatenate them along the channel to obtain an audio-visual representation with dimension of $T \times H \times W \times 2D$. This representation is fed

Methods	Ego4D			Aria		
	F1	Rec.	Prec.	F1	Rec.	Prec.
STS + Vanilla Contr	39.0	53.7	30.6	59.1	66.5	53.1
STS + S-Contr	38.5	53.5	30.0	59.0	66.3	53.1
STS + T-Contr	38.9	54.0	30.5	59.0	66.7	53.0
STS + Cross Contr	38.9	54.4	30.2	59.3	66.8	53.3
STS + Post Contr	39.7	53.3	31.6	59.9	66.8	54.3

Table 5. Study of different strategies for contrastive loss implementation. The best results are highlighted with **boldface**. The highlighted row refers to the complete CSTS model. See Section C for further discussion.

into the decoder for gaze forecasting.

Vanilla SA. In this baseline, we flatten the video embedding and audio embedding into a list of tokens and thereby obtain $T \times (N + M)$ tokens in total, where $N = H \times W$. Then we input all tokens to a standard self-attention layer followed by multiple linear layers to perform fusion in the spatial and temporal dimensions simultaneously. We split the output into a new visual embedding incorporating audio information with dimension of $T \times N \times D$ and a new audio embedding incorporating visual information with dimension of $T \times M \times D$. The new visual embedding is input into the decoder.

Seq. ST. We implement a sequential variant of our proposed fusion strategy. The visual and audio embeddings are fed into the temporal fusion module first and then go through the spatial fusion module. Specifically, we input $\phi(x)$ and $\psi(a)$ into the temporal fusion module and obtain the output $u_{v,t}$ and $u_{a,t}$. We also use $u_{a,t}$ to reweight $\psi(a)$ resulting in $u_a \in \mathbb{R}^{T \times M \times D}$ as discussed in Section 3.2 and 3.3 from the main paper. For the visual embeddings, we use $u_{v,t}$ to reweight $\phi(x)$ and obtain a new reweighted visual embedding, *i.e.* $\hat{u}_v = \phi(x) \otimes u_{v,t} \in \mathbb{R}^{T \times H \times W \times D}$. \hat{u}_v and u_a serve as the input to the spatial fusion module. Then, we further generate a new visual representation incorporating audio information from the spatial fusion module and input the resulting embedding into the decoder.

STS. This is a baseline using the same fusion strategy as our method but without using the contrastive loss for training.

C. Experiments on Contrastive Learning

In our model, we propose to use the audio-visual representations obtained after fusion (*i.e.* u_v and u_a) to calculate contrastive loss. As a comparison, we also implement a baseline by feeding the raw embeddings from the encoders (*i.e.* $\phi(x)$ and $\psi(a)$) to the contrastive loss which is denoted as **Vanilla Contr**. To further investigate the contribution

of contrastive learning, we also conduct experiments with three additional strategies:

Cross Contr. In our final model (CSTS), we use the new visual representation $u_v = u_{v,s} \otimes u_{v,t}$ and the new audio representation $u_a = \psi(a) \otimes u_{a,t}$ as input to the contrastive loss. In Cross Contr, we still use u_v yet replace u_a by reweighting the audio representation $u_{a,s}$ after the spatial fusion with weight $u_{a,t}$ from the temporal fusion, *i.e.* $u_a^* = u_{a,s} \otimes u_{a,t}$, as input to the contrastive loss. Please refer to Fig. 2 in the main paper for the meaning of each notation.

S-Contr. We use the output from the spatial fusion module ($u_{v,s}, u_{a,s}$) to calculate the contrastive loss.

T-Contr. We use the output from the temporal fusion module ($u_{v,t}, u_{a,t}$) to calculate the contrastive loss.

We implement all contrastive learning baselines above on our proposed model architecture and fusion strategy (*i.e.* STS). The results are summarized in Table 5. Both S-Contr and T-Contr lag behind or perform on par with Vanilla Contr. One possible reason is that conducting contrastive learning using features obtained from only one fusion branch may compromise the representation learning of the other branch. Additionally, Cross Contr works on-par with Vanilla Contr on Ego4D but performs better on Aria. It also consistently outperforms S-Contr and T-Contr. This result validates our claim that implementing contrastive loss with reweighted representations from both spatial and temporal fusion leads to more gains for egocentric gaze anticipation. Moreover, our proposed strategy (reweighting the raw audio embedding $\psi(a)$ rather than the fused embedding after spatial fusion) outperforms Cross Contr. This is because in Cross Contr $u_{a,s}$ is derived from spatial fusion, where each audio token is fused with 64 visual tokens in the spatial fusion branch resulting in the dilution of audio features. All results further demonstrate the benefits of our proposed contrastive learning strategy.

D. Results on Egocentric Gaze Estimation

In addition to egocentric gaze anticipation, we also evaluate the generalization capability of our proposed method by conducting experiments on the separate egocentric gaze estimation problem using our model design. We use the same experiment setup from the recent state-of-the-art method [33] in egocentric gaze estimation.

As demonstrated in Table 6, previous work [33] has shown the superiority of using a transformer-based architecture for egocentric gaze estimation. By incorporating the audio modality, CSTS surpasses the backbone MViT [12] (vision-only counterpart) by +2.8% on both Ego4D and Aria in terms of F1. These results indicate the audio modality makes important contributions to the performance on egocentric gaze estimation. Furthermore, our model outperforms GLC [33] by +0.6% and +1.3% on Ego4D and Aria respectively, achieving a new state-of-the-art performance

Methods	Ego4D			Aria		
	F1	Rec.	Prec.	F1	Rec.	Prec.
Center Prior	14.9	21.9	11.3	28.9	21.7	43.1
GazeMLE [35]	35.4	49.7	27.5	58.7	63.4	54.7
AttnTransit [24]	36.4	47.6	29.5	59.2	60.2	58.3
I3D-R50 [13]	37.5	52.5	29.2	60.9	69.5	54.2
MViT [12]	40.9	57.4	31.7	61.7	71.2	54.5
GLC [33]	43.1	57.0	34.7	63.2	67.4	59.5
CSTS	43.7	58.0	35.1	64.5	69.6	60.1

Table 6. Comparison with previous state-of-the-art models on egocentric gaze estimation. The best results are highlighted with **bold-face**. See Section D for further discussion.

for this problem. However, our method has a smaller performance improvement on the gaze estimation task compared to gaze anticipation. We speculate that this is because a person typically orients their gaze in response to audio signals, so there is usually a delay between audio and correlated gaze movement. The audio thus has a stronger connection with future gaze targets.

E. Additional Visualization

We showcase further qualitative comparisons with all the baselines for egocentric gaze anticipation in Fig. 6. We observe CSTS makes the most accurate predictions. We also illustrate some typical failure cases in Fig. 7. In the first example, our model makes an accurate prediction in the first frame but fails at the following time steps due to the gaze movement. In the second example, the the camera view and gaze target move from the left to the right. This drastic change causes the mistake in our model’s predictions. Similar failures also happen in the predictions of all baselines. Notably, existing deep models tend to only successfully anticipate steady gaze fixations or small gaze movements in the near future, and can not effectively capture large gaze shifts. This is the a common limitation shared by many existing works of future anticipation [28] in egocentric videos.

F. Limitation and Future Work

In this paper, we propose a novel contrastive spatial-temporal separable fusion model for audio-visual egocentric gaze anticipation. Our method is validated on the Ego4D [17] and Aria [29] datasets. Our method has larger performance improvement on the Aria dataset comparing with Ego4D dataset. We believe this is because the multi-person social interaction setting from Ego4D dataset incurs additional challenges for audio representation learning, like multiple people and speakers present. Our current model design did not explicitly address this challenging nature of multi-speaker social interactions. Another limitation is that our model fails to anticipate the drastic gaze movements

(see the failure cases in Fig. 7). In addition, in this work we do not explore the spatial geometry context provided by multi-channel audio signals. Our approach and experiments suggest several important future research directions:

- The proposed CSTS model can be applied to other video understanding tasks related to the audio modality, such as action recognition, action localization, and video question answering. We hope to further investigate our proposed approach on these problem settings.
- A model explicitly designed for audio-visual representation learning in multi-person, multi-speaker environments merits further investigation.
- A model that learns better temporal representations for anticipating large gaze shifts remains to be explored.
- The visualization of correlation weights in the spatial fusion module indicates the potential of our model for weakly-supervised/self-supervised sound localization and active speaker detection, which can be investigated in further work.

G. Code and License

The usage of the Aria Dataset is under the Apache 2.0 License², and the usage of the Ego4D Dataset is under the license agreement³. Our implementation is built on top of [11], which is under the Apache License⁴. Our code and the train/test split on Aria dataset will be available at: <https://www.anonymous-for-review.com>.

²<https://github.com/facebookresearch/vrs/blob/main/LICENSE>

³<https://ego4d-data.org/pdfs/Ego4D-Licenses-Draft.pdf>

⁴<https://github.com/facebookresearch/SlowFast/blob/main/LICENSE>

	Stages	Operators	Output Size
Video Encoder $\phi(x)$	video frames	-	$8 \times 256 \times 256 \times 3$
	video token embedding	$Conv(3 \times 7 \times 7, 96)$ <i>stride</i> $2 \times 4 \times 4$	$4 \times 64 \times 64 \times 96$
	tokenization	flattening	$(4 \times 64 \times 64) \times 96$
	video encoder block1	$\begin{bmatrix} MSA(96) \\ MLP(384) \end{bmatrix} \times 1$	$(4 \times 64 \times 64) \times 192$
	video encoder block2	$\begin{bmatrix} MSA(192) \\ MLP(768) \end{bmatrix} \times 2$	$(4 \times 32 \times 32) \times 384$
	video encoder block3	$\begin{bmatrix} MSA(384) \\ MLP(1536) \end{bmatrix} \times 11$	$(4 \times 16 \times 16) \times 768$
	video encoder block4	$\begin{bmatrix} MSA(768) \\ MLP(3072) \end{bmatrix} \times 2$	$(4 \times 8 \times 8) \times 768$
Audio Encoder $\psi(a)$	audio spectrograms	-	$8 \times 256 \times 256 \times 1$
	audio token embedding	$Conv(3 \times 7 \times 7, 96)$ <i>stride</i> $2 \times 4 \times 4$	$4 \times 64 \times 64 \times 96$
	tokenization	flattening	$(4 \times 64 \times 64) \times 96$
	audio encoder block1	$\begin{bmatrix} MSA(96) \\ MLP(384) \end{bmatrix} \times 1$	$(4 \times 4096) \times 192$
	audio encoder block2	$\begin{bmatrix} MSA(192) \\ MLP(768) \end{bmatrix} \times 1$	$(4 \times 1024) \times 384$
	audio encoder block3	$\begin{bmatrix} MSA(384) \\ MLP(1536) \end{bmatrix} \times 1$	$(4 \times 256) \times 768$
	audio encoder block4	$\begin{bmatrix} MSA(768) \\ MLP(3072) \end{bmatrix} \times 1$	$(4 \times 64) \times 768$
Fusion Modules	conv1	$Conv(768 \times 1 \times 8 \times 8, 768)$ <i>stride</i> $1 \times 1 \times 1$	$4 \times 1 \times 768$
	in-frame self-attention $\sigma(\cdot)$	$\begin{bmatrix} MSA(768) \\ MLP(3072) \end{bmatrix} \times 1$	$4 \times (64 + 1) \times 768$
	conv2	$Conv(768 \times 1 \times 8 \times 8, 768)$ <i>stride</i> $1 \times 1 \times 1$	$4 \times 1 \times 768$
	conv3	$Conv(768 \times 1 \times 8 \times 8, 768)$ <i>stride</i> $1 \times 1 \times 1$	$4 \times 1 \times 768$
	cross-frame self-attention $\pi(\cdot)$	$\begin{bmatrix} MSA(768) \\ MLP(3072) \end{bmatrix} \times 1$	$8 \times 1 \times 768$
	reweighting	$u_{v,s} \otimes u_{v,t}$	$8 \times 64 \times 768$
	reweighting	$\psi(a) \otimes u_{a,t}$	$8 \times 64 \times 768$
Decoder	decoder block1	$\begin{bmatrix} MSA(1536) \\ MLP(3072) \end{bmatrix} \times 1$	$(4 \times 16 \times 16) \times 768$
	decoder block2	$\begin{bmatrix} MSA(768) \\ MLP(1536) \end{bmatrix} \times 1$	$(4 \times 32 \times 32) \times 384$
	decoder block3	$\begin{bmatrix} MSA(384) \\ MLP(768) \end{bmatrix} \times 1$	$(4 \times 64 \times 64) \times 192$
	decoder block4	$\begin{bmatrix} MSA(192) \\ MLP(384) \end{bmatrix} \times 1$	$(8 \times 64 \times 64) \times 96$
	head	$Conv(1 \times 1 \times 1, 1)$ <i>stride</i> $1 \times 1 \times 1$	$8 \times 64 \times 64 \times 1$

Table 7. Architecture of the proposed model. Convolutional layers are denoted as $Conv(kernel\ size, output\ channels)$. The number of input channels in multi-head self-attention is shown in the parenthesis of MSA . The dimension of the hidden layer in multi-layer perceptron is listed in parenthesis of MLP . conv1 is the convolutional layer in the spatial fusion module. conv2 and conv3 are convolutional layers in the temporal fusion module.

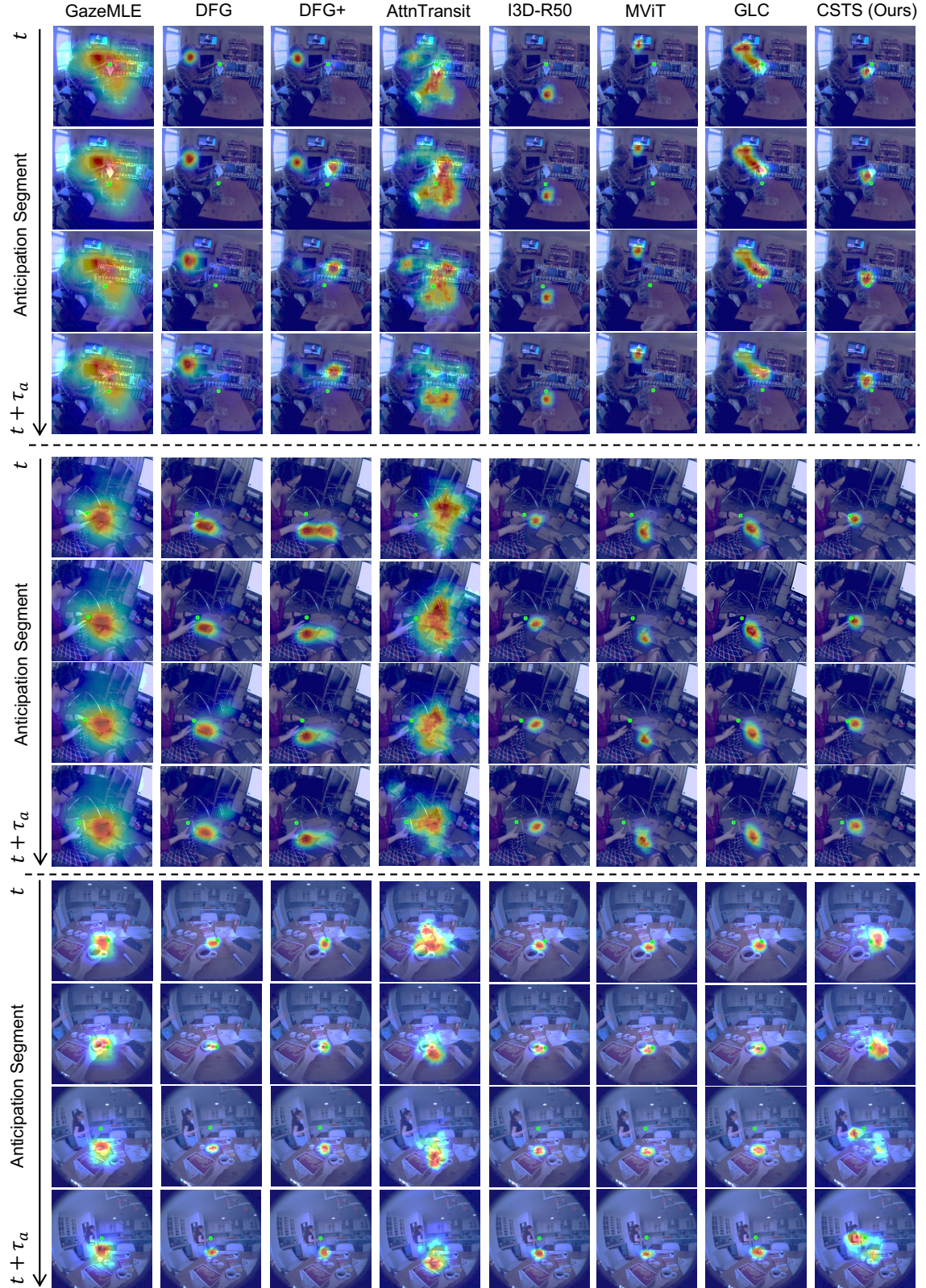


Figure 6. Additional egocentric gaze anticipation results from our model and other baselines. **Green dots** indicate the ground truth gaze location. The first two examples are from the Ego4D dataset, and the last example is from the Aria dataset.

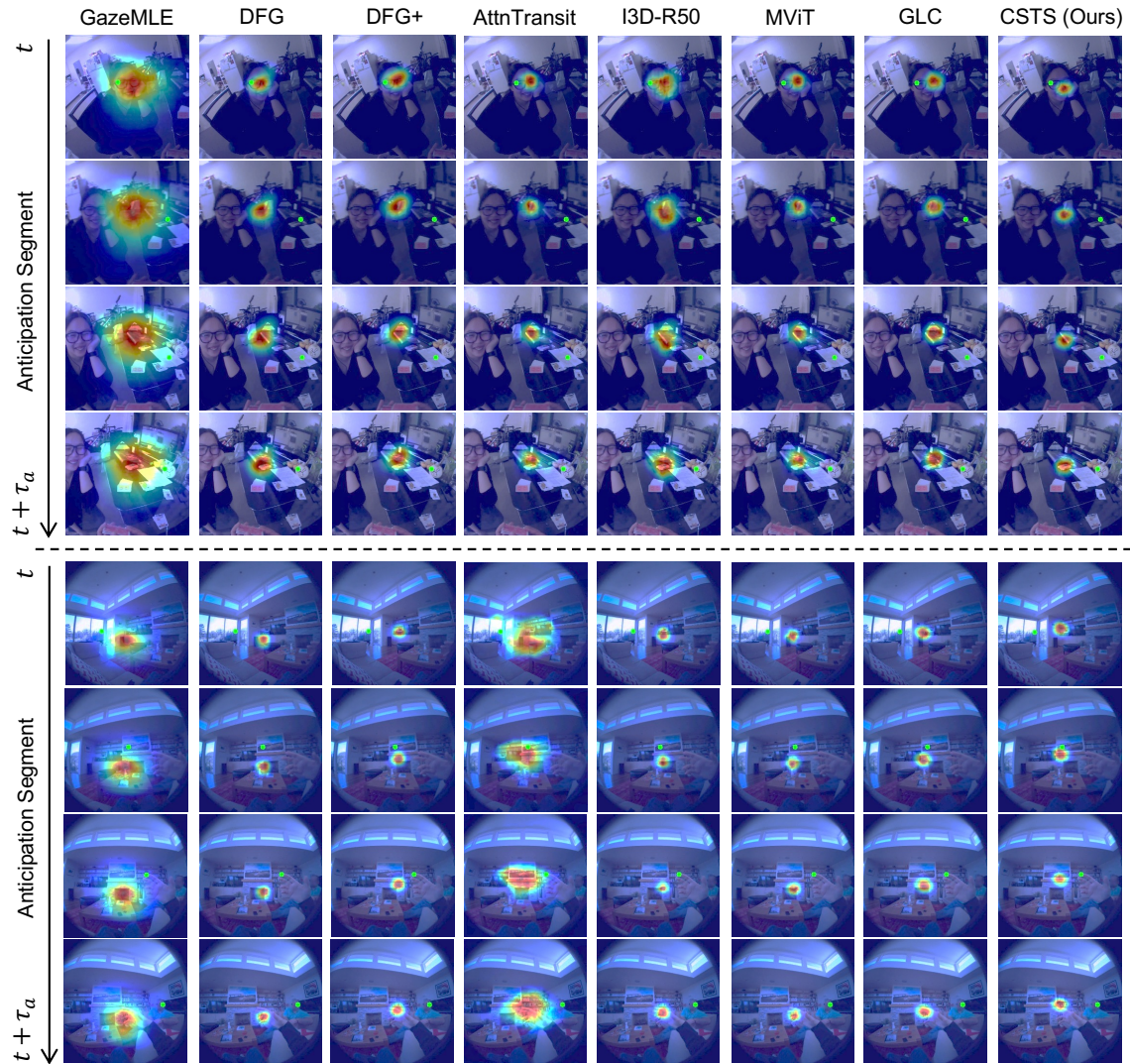


Figure 7. Failure cases of our model and baselines. **Green dots** indicate the ground truth gaze location. The first example is from the Ego4D dataset, and the second example is from the Aria dataset.